NANO LETTERS

pubs.acs.org/NanoLett Letter

Structural Anisotropy-Driven Atomic Mechanisms of Phase Transformations in the Pt−Sn System

Hwanhui Yun,* Delin Zhang, Turan Birol, Jian-Ping Wang, and K. Andre Mkhoyan*

Cite This: *Nano Lett.* 2023, 23, 7576−7583 Read Online

ACCESS | Metrics & More | Article Recommendations | Supporting Information

ABSTRACT: Using *in situ* atomic-resolution scanning transmission electron microscopy, atomic movements and rearrangements associated with diffusive solid to solid phase transformations in the Pt−Sn system are captured to reveal details of the underlying atomistic mechanisms that drive these transformations. In the $PtSn_4$ to $PtSn_2$ phase transformation, a periodic superlattice substructure and a unique intermediate structure precede the nucleation and growth of the $PtSn_2$ phase. At the atomic level, all stages of the transformation are templated by the anisotropic crystal structure of the parent $PtSn_4$ phase. In the case of the $PtSn_2$ to Pt_2Sn_3 transformation, the anisotropy in the structure of product Pt_2Sn_3 dictates the path of transformation. Analysis of atomic configurations at the transformation front elucidates the diffusion pathways and lattice distortions required for these phase transformations. Comparison of multiple Pt−Sn phase transformations reveals the structural parameters governing solid to solid phase transformations in this technologically interesting intermetallic system.

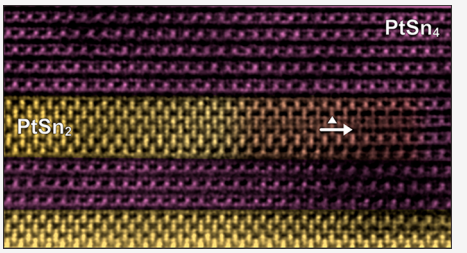

KEYWORDS: *$PtSn_4$, $PtSn_2$, Pt_2Sn_3, in situ STEM, atomic resolution, phase transformation*

Over the past two decades, interest in better understanding solid to solid phase transformations, particularly in nanomaterials, has grown considerably due to the potential for tuning their mechanical, catalytic, and electronic properties.[1−4] In these solid to solid phase transformations—driven by temperature, pressure, or other stimuli[5−7]—the transitions are either purely structural (martensitic) or combined structural and compositional (diffusive).[8−10] The latter type, involving long-range movements of the atoms in the system that can proceed at an adjustable speed, is both more desirable and more difficult to study. In nanoscale materials, these transformations are sometimes accompanied by the formation of unexpected polymorphs and intermediate structures[11−17] that further complicate the pathway. To effectively control these diffusive solid to solid phase transformations, understanding the underlying atomistic mechanisms that dictate the transition pathway between the product and parent phases is critical and needs direct measurements. Therefore, developing atomic-level experimental methods for characterizing transitional stages in these diffusive solid to solid phase transformations, as they happen, is necessary to gain insight into the key factors driving these phase transformations. Combining *in situ* and *ex situ* atomic-resolution measurements using analytical aberration-corrected scanning transmission electron microscopy (STEM) satisfies requirements for such measurements and has been shown to be effective for studying martensitic phase transformation.[18,19] Here, we employed direct STEM imaging[13,16−18,20] and diffraction[21] to study local structure and crystallographic orientations and spatially resolved energy dispersive x-ray (EDX) spectroscopy[15,22,23] to determine the composition of intermediate structures and phases.

In this work, we adapted analytical atomic-resolution STEM for *in situ* measurements to shed new light on the atomistic mechanisms of solid to solid phase transformations in the Pt−Sn system,[24,25] going step by step from $PtSn_4$ to $PtSn_2$, then from $PtSn_2$ to Pt_2Sn_3, and, finally, from $PtSn_2$ to PtSn. These include transformations from highly anisotropic, layered, orthorhombic $PtSn_4$ to isotropic cubic $PtSn_2$ and then to another layered hexagonal Pt_2Sn_3. Atomic rearrangements captured by STEM imaging and spectroscopy showed a direct correlation between the type of anisotropy present in the crystal structure of either parent or product phase and the pathway involved in transforming to the product phase. Because the individual phases of the Pt−Sn system are still challenging to grow, especially in the form of thin films and nanoparticles[20,26] needed for applications in catalysis and spintronics,[27−30] successive solid to solid phase transformations discussed here serve as a promising alternative to direct synthesis.[4,7]

Received: June 8, 2023
Revised: July 19, 2023
Published: August 3, 2023

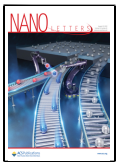

https://doi.org/10.1021/acs.nanolett.3c02162
Nano Lett. 2023, 23, 7576−7583

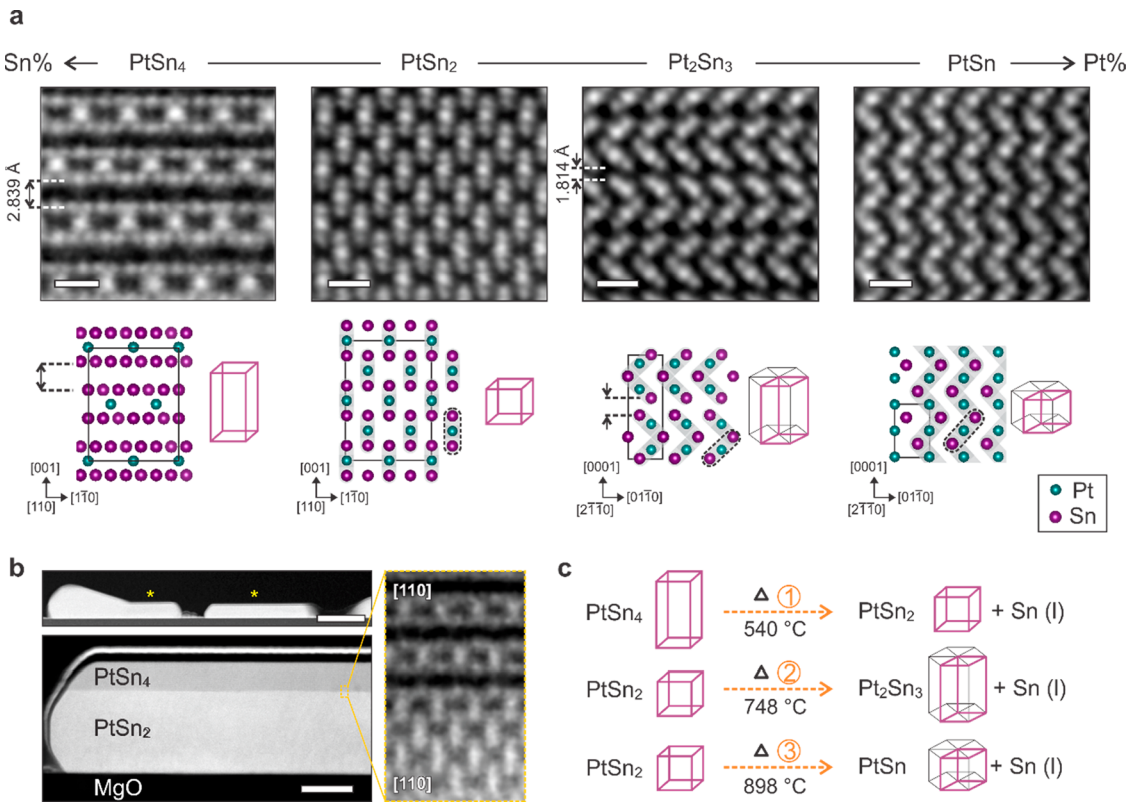

Figure 1. (a) High-resolution HAADF-STEM images of the four Pt_xSn_y phases discussed in this study. Scale bars are 5 Å. Atomic models and crystal lattice structures are illustrated below the HAADF-STEM images. Structural gaps in two-dimensional-like $PtSn_4$ and Pt_2Sn_3 are marked with dashed lines. Color codes for the atomic models: cyan for Pt and magenta for Sn. (b) Cross-sectional low- and medium-magnification HAADF-STEM images of an initial $PtSn_4/PtSn_2$ lamella grown on a MgO substrate. Scale bars are 500 nm (top) and 50 nm (bottom). A high-resolution image of the $PtSn_2/PtSn_4$ interface is presented on the right, showing the atomic structure of the interface. See Figure S1 for the EDX maps of the interface. (c) Simple schematic of three phase transformations (①, ②, and ③) among these four Pt_xSn_y phases, including their known bulk transition temperatures.[25]

RESULTS

In Figure 1a, the atomic-resolution HAADF-STEM images are presented in order of a decreasing Sn/Pt atomic ratio. While the phases all exhibit clearly distinct crystal structures, they share an important resemblance that influences diffusive transformations among them. $PtSn_4$ has an orthorhombic crystal structure with space group *Ccee* (No. 68). It consists of layers separated with large 2.839 Å[31] gaps along the [001] direction, which are clearly visible when viewed perpendicular to that direction. Each unit cell of $PtSn_4$ includes two such layers, with each layer composed of a Pt{0001} plane sandwiched between two Sn{0001} planes. $PtSn_2$ has a cubic structure with space group $Fm\bar{3}m$ (No. 225). While higher-symmetry $PtSn_2$ seems drastically dissimilar to lower-symmetry $PtSn_4$, note that introducing additional Pt atoms into the gaps in $PtSn_4$ results in a structure similar to that of $PtSn_2$; this is an important structural relationship that is discussed further below. Pt_2Sn_3 and PtSn both have hexagonal structures with space group $P6_3/mmc$ (No. 194). While these two phases exhibit seemingly very similar atomic configurations, seen in the atomic-resolution images and crystal structure diagrams in Figure 1a, lower-symmetry Pt_2Sn_3 has 1.814 Å[32] interlayer gaps perpendicular to the [0001] direction that are absent in PtSn. Note the interesting similarity among the atomic structures of $PtSn_2$, Pt_2Sn_3, and PtSn. A common Sn−Pt−Sn (SPS) elemental building unit is present in each of them, corresponding to nearly identical bonding configurations in the SPS units across all three phases (Figure S1). Each of the four phases studied possesses unique convergent beam electron diffraction (CBED) patterns and electron energy-loss spectroscopy (EELS) spectra (Figures S2 and S3), which were employed to identify phases during *in situ* STEM heating experiments whenever atomic-resolution imaging was not possible.

The Pt_xSn_y film used for this study consists of islands that are composed of $PtSn_4$ and $PtSn_2$ phases, and $PtSn_4/PtSn_2$ lamella-structured islands were chosen for phase transformation experiments. See section S1 of the Supporting Information for details. Starting from a $PtSn_4/PtSn_2$ lamella, three types of phase transformations were studied: ① $PtSn_4$ to $PtSn_2$, ② $PtSn_2$ to Pt_2Sn_3, and ③ $PtSn_2$ to PtSn (Figure 1c). For each of the three diffusive phase transformations, we determine the atomistic mechanism and crystallographic orientation relationship (OR) characteristic of that transformation. Quantitative characterization of transformation kinetics (e.g., reaction rates, diffusion rates of atoms, and exact transition temperatures) is outside the scope of this study.

$PtSn_4$ to $PtSn_2$ (layered orthorhombic to cubic) Phase Transformation. To examine the transformation from $PtSn_4$ to $PtSn_2$, $PtSn_4/PtSn_2$ lamellae were gradually heated inside the transmission electron microscope (Figure 2a and Video S1). As the temperature reaches 250 °C, a dark lateral stripe contrast arises in the $PtSn_4$ region and expands because of transformation to the $PtSn_2$ phase. Propagation of product $PtSn_2$ is faster along the horizontal ⟨110⟩ directions than along

https://doi.org/10.1021/acs.nanolett.3c02162
Nano Lett. 2023, 23, 7576−7583

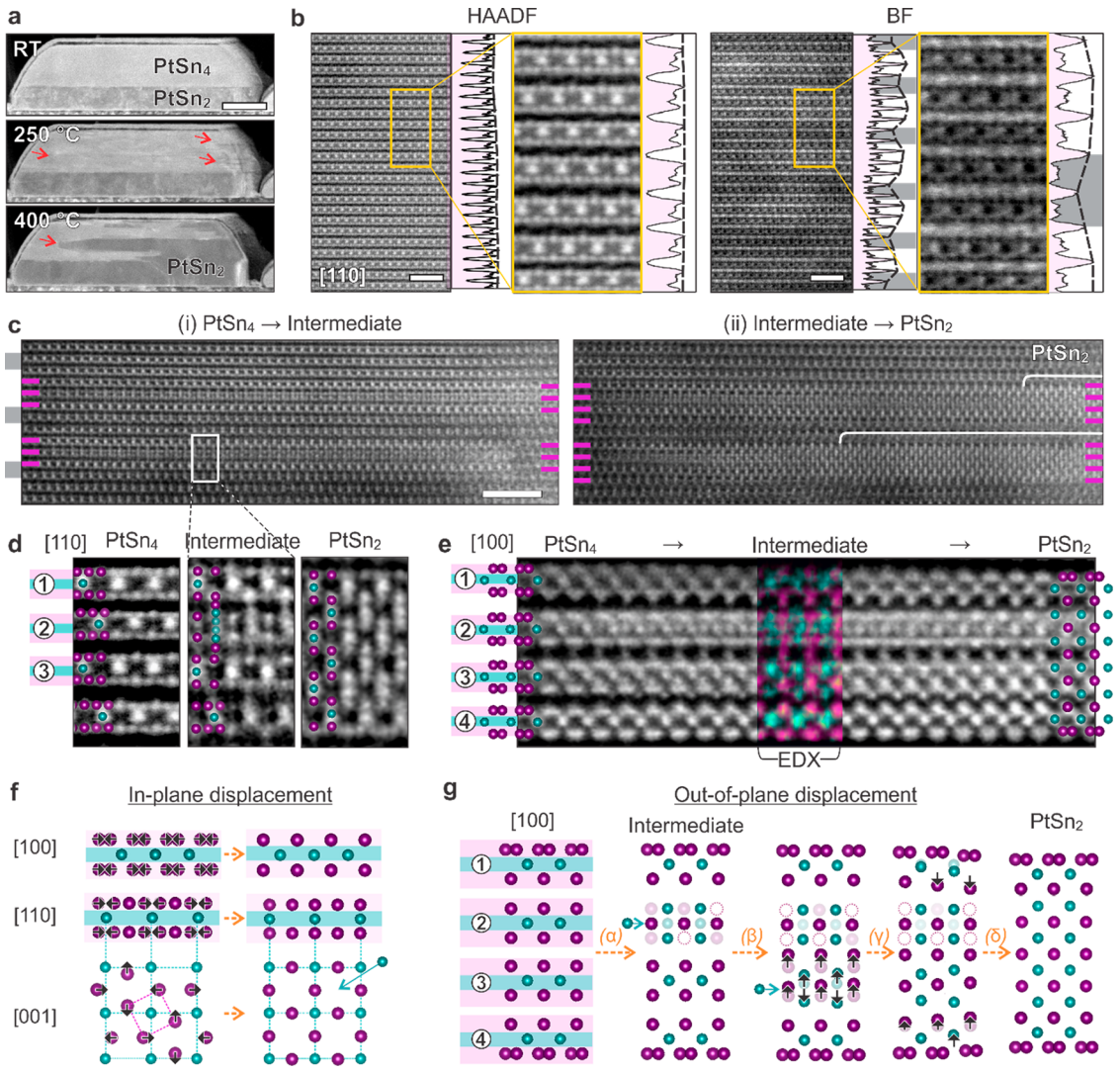

Figure 2. Nucleation stage in the $PtSn_4$to $PtSn_2$ phase transformation. (a) *In situ* $PtSn_4$ to $PtSn_2$ phase transformation captured in a series of STEM images. LAADF-STEM is used here to enhance the contrast between the two phases. The growth of $PtSn_2$ in the $PtSn_4$ region is marked with red arrows. The scale bar is 100 nm. (b) HAADF- and BF-STEM images of $PtSn_4$ at 150 °C viewed along the [110] direction. The insets show magnified images from the region inside the yellow boxes. Intensity line profiles are plotted to the right of each image, highlighting the emergence of lateral stripe contrast in the BF-STEM images. Scale bars are 2 nm. (c) Pair of HAADF-STEM images showing the initial stages of the $PtSn_4$ to $PtSn_2$ phase transition at 210 °C. The scale bar is 3 nm. (i) Emergence of three-layer-thick (highlighted with magenta lines) intermediate phases in $PtSn_4$. The position of the layers with a dark contrast in BF-STEM is indicated with shaded gray lines on the left. (ii) Evolution of the intermediate phase into $PtSn_4$. Four-layer $PtSn_4$ regions that transform into $PtSn_2$ are marked with magenta lines. (d) Comparison of the $PtSn_4$, intermediate, and $PtSn_2$ phases from HAADF-STEM images in the [110] direction with overlaid atomic models (cyan for Pt and magenta for Sn). (e) HAADF-STEM image capturing the phase evolution from $PtSn_4$ to $PtSn_2$ viewed from the [100] projection. EDX elemental maps are overlaid in the region of the intermediate phase. The image is compared with HAADF-STEM images from bulk $PtSn_4$ and $PtSn_2$ in Figure S5. Schematics describe (f) in-plane and (g) out-of-plane atomic displacements during the $PtSn_4$ to $PtSn_2$ phase transition. Orange arrows indicate the change in the structure due to phase transformation, and black arrows on the atoms represent the associated atomic displacements. The cyan arrows with Pt atomic models indicate the suggested Pt diffusion pathway. Sn vacancies at layer ② are depicted with white circles with a magenta line color. Out-of-plane displacements are described by a combination of four unique displacement behaviors.

the [001] direction, as evidenced by the laterally stretched contrast in the STEM images. At ∼540 °C, in addition to the previously formed $PtSn_2$, a liquid Sn region develops near the edge of the island (Figure S4). Eventually, all of the $PtSn_4$ transforms into $PtSn_2$ and liquid Sn. The liquid Sn solidifies into β-Sn, if the sample is cooled to room temperature (RT), but it vaporizes when heated above 540 °C. The crystallographic OR of the $PtSn_4$ to $PtSn_2$ phase transformation is $PtSn_4(001)\|PtSn_2(001)$ and $PtSn_4\langle 110\rangle\|PtSn_2\langle 110\rangle$, according to CBED data (Figure S4). The product $PtSn_2$ phase grows faster along the in-plane direction of the coherent planes.

To investigate the atomic mechanism of the phase transformation, a phase transition was initiated by slowly heating a $PtSn_4/PtSn_2$ lamella from RT to 300 °C (Video S2). First, at 150 °C, structural modulations develop in parent $PtSn_4$. These modulations are subtle, resulting in no contrast change in HAADF-STEM images. However, they are clearly visible in bright-field (BF) STEM images as lateral dark contrasts appearing once every four to five $PtSn_4$ layers (Figure 2b and Figure S5). This periodic contrast is also visible in high-magnification BF-STEM images obtained from the other main in-plane [100] direction (Figure S5). This periodic feature

https://doi.org/10.1021/acs.nanolett.3c02162
Nano Lett. 2023, 23, 7576−7583

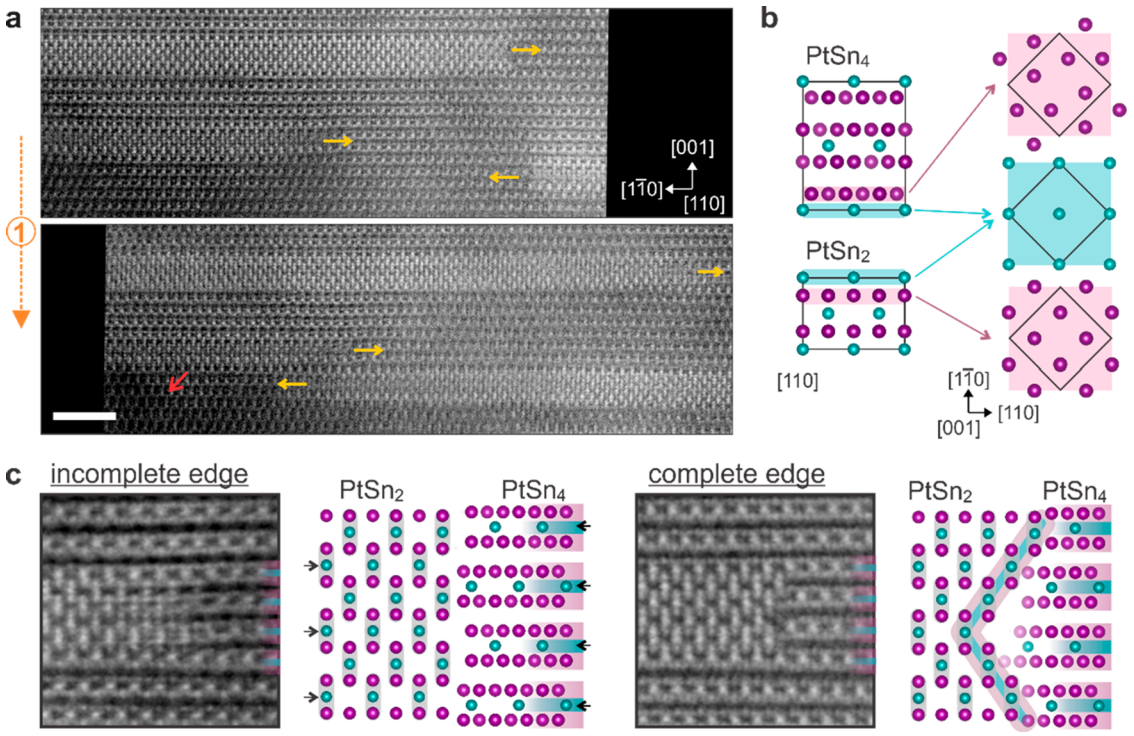

Figure 3. (a) Pair of HAADF-STEM images showing the growth of $PtSn_2$ slabs in $PtSn_4$. The growth direction of each slab is indicated by yellow arrows located on the propagation front. A depleted region with a dark contrast is indicated by the red arrow. The scale bar is 3 nm. (b) Atomic models showing the common Pt{001} and semicoherent Sn{001} planes in $PtSn_2$ and $PtSn_4$. (c) HAADF-STEM images and corresponding atomic models of incomplete and complete edges of the propagation front of a $PtSn_2$ slab in a $PtSn_4$ matrix. Pt diffusion paths are indicated by black arrows. The complete edge between two phases corresponds to a set of $PtSn_2${112} planes, which are marked with shaded lines.

remains the same when the sample is cooled from 150 °C to RT, indicating a permanent change in the structure. We speculate that this periodic contrast in the BF (not visible in HAADF) images stems from periodic strain in the structure resulting from ordered vacancy formation (mostly lighter Sn vacancies), producing an enlarged superlattice that can be readily accommodated in layered $PtSn_4$. Similar two-dimensional (2D)-like structural modulations at increased temperatures have been observed in In_2Se_3.[33]

At ~200 °C, a new intermediate phase appears in the layers between the dark bands of the BF-STEM image; the intermediate phase develops into $PtSn_2$ upon further heating (Figure 2c and Figure S5). The intermediate phase exhibits an atomic structure that is different not only from those of the parent ($PtSn_4$) and product ($PtSn_2$) phases but also from those of any existing Pt_xSn_y phases. It is confined within three $PtSn_4$ layers (①–③ in Figure 2d) and spans laterally. The HAADF-STEM image and EDX elemental maps of this intermediate phase (Figure 2d and Figure S5) reveal major atomic rearrangement in the middle layer ② and minor changes in the two capping layers, ① and ③. The atomic modifications needed for the formation of the intermediate phase from $PtSn_4$ can be described by a combination of in-plane and out-of-plane displacements, as depicted schematically in panels f and g of Figure 2. Whereas in-plane displacement of Sn atoms (which transforms a Sn{001} plane in $PtSn_4$ into a Sn{001} plane of $PtSn_2$) occurs in all three layers, the atomic movements in the out-of-plane direction are distinct in each layer. Out-of-plane displacement of Pt atoms occurs only in the middle layer, ②, where a Pt{001} plane splits into two Pt{001} planes (step α in Figure 2g). Here, Pt is supplemented via in-plane atomic influx, which can be deduced from the unaltered contrast of the neighboring ① and ③ layers, and Sn atoms seem to diffuse along the in-plane direction generating Sn vacancies. Similar out-of-plane atomic displacements occurring at lower temperatures, albeit far more subtle, may account for the periodic feature captured in BF-STEM images at 150 °C.

Next, the three-layer-thick intermediate phase interacts with one adjacent $PtSn_4$ layer to transform into $PtSn_2$. Such evolution of atomic rearrangements from $PtSn_4$ to the intermediate phase and to the $PtSn_2$ phase was captured in a single HAADF-STEM image (Figure 2e). The in-plane displacement of Sn atoms observed in the intermediate phase also occurred in all remaining layers except for the two outermost boundary Sn{001} planes. Along with the out-of-plane Pt splitting in layer ② from the intermediate phase formation (step α), the Pt{001} plane in layer ③ also splits in the out-of-plane direction, generating two Pt{001} planes (Figure 2g). Simultaneously, out-of-plane shifts of Sn{001} planes toward the center of layer ② occur in all of the layers (β–δ step). Eventually, four layers of $PtSn_4$ turn into a 1.5-unit cell (6-Pt{001}-plane-thick) $PtSn_2$ slab. Note that such a transformation requires diffusion of additional Pt into the matrix along with the removal of Sn. Pt diffuses into layers ② and ③ primarily within the Pt{001} layer along the in-plane direction. As one can see in the atomic models from the [001] direction, the Pt{001} plane is less densely packed than the Sn{001} plane and has some vacant positions, which can be used as the diffusion pathway. Darker patches with a modified atomic configuration are observed near the edge of the new $PtSn_2$ slabs, indicating formation of Pt-depleted regions after the diffusion of Pt into the $PtSn_2$ phase (Figure 3a). Sn atoms diffuse out to the lateral surface primarily along the in-plane

https://doi.org/10.1021/acs.nanolett.3c02162
Nano Lett. 2023, 23, 7576–7583

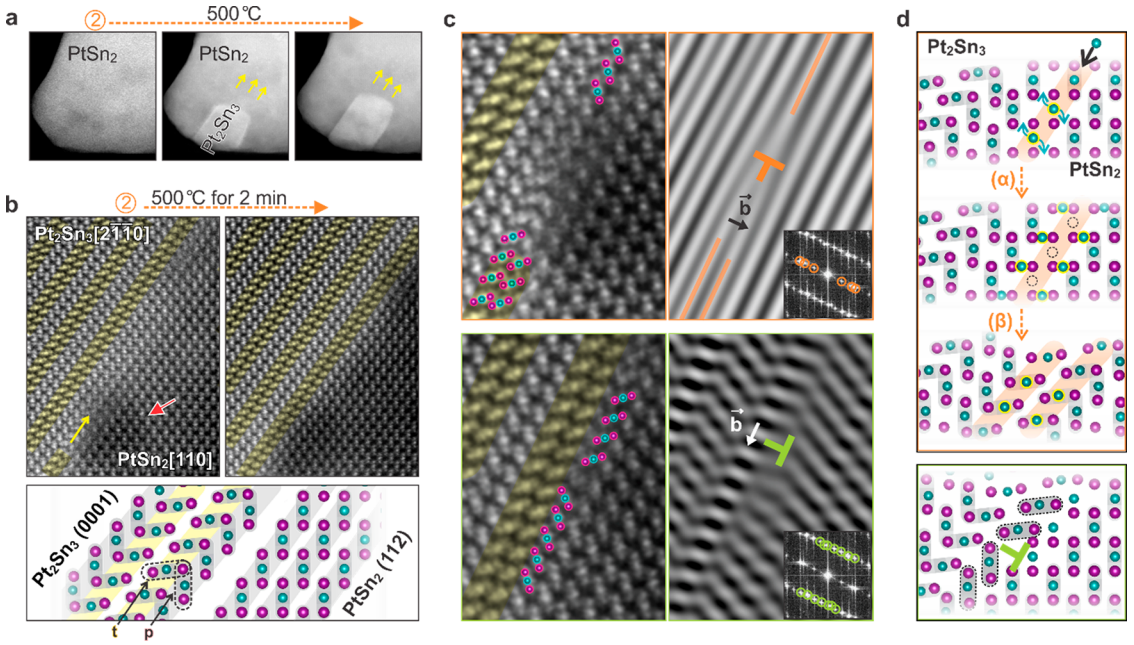

Figure 4. $PtSn_2$ to Pt_2Sn_3 phase transformation. (a) Set of *in situ* HAADF-STEM images showing the formation and growth of Pt_2Sn_3 in $PtSn_2$. (b) Atomic-resolution HAADF-STEM images showing the growth of a layer of Pt_2Sn_3 at the $PtSn_2/Pt_2Sn_3$ boundary. Atomic models of the $Pt_2Sn_3/PtSn_2$ interface are included at the bottom, where two types of SPS configurations in Pt_2Sn_3 are outlined with black dashed lines and labeled as p (for parallel) and t (for tilted). The Pt_2Sn_3 layer growth direction is indicated by the yellow arrow, and a depleted region with dark contrast is indicated by the red arrow. $Pt_2Sn_3\{0001\}$ planes composed of t-type SPS are highlighted in yellow. (c) HAADF-STEM images of type 1 (top) and type 2 (bottom) edge dislocations at the $PtSn_2-Pt_2Sn_3$ interface with the Burgers vector perpendicular and parallel to the interface, respectively. Fourier-filtered images on the right show the location of dislocations (insets, used Fourier spots). (d) Schematics describing the role of the two dislocations in transforming the p-type SPS units into t-type units at the $PtSn_2-Pt_2Sn_3$ interface.

direction, as liquid Sn regions form only at the side face of the original $PtSn_4$ region, not at the top or bottom (Video S1).

As the phase transformation progresses, the 1.5-unit cell $PtSn_2$ slab expands along the in-plane direction in the $PtSn_4$ matrix while sandwiched between the $PtSn_4\{001\}-PtSn_2\{001\}$ interfaces (Figure 3a and Video S3). Such anisotropic growth is favorable, owing to the presence of a coherent $PtSn_4(001)\|PtSn_2(001)$ interface as well as the layered structure of $PtSn_4$. As illustrated in Figure 3b, these two phases possess identical Pt{001} atomic planes and similar Sn{001} planes with a negligible in-plane lattice mismatch (<0.4%), which contributes to the stability of the interface. The large gaps in the layered structure of $PtSn_4$ provide a buffer in interaction with the neighboring layers and flexibility in the atomic displacements for $PtSn_2$ formation. Furthermore, the thickness of the 1.5-unit cell $PtSn_2$ slab (1.934 nm)[34] is comparable to the thickness of the four layers of $PtSn_4$ (1.987 nm),[31] which further stabilizes the configuration. The layered structure of $PtSn_4$ dictates every aspect of this phase transformation, including the emergence of the intermediate phase, stabilization of homogeneous nuclei, and directional growth of the product $PtSn_2$ phase.

Once the nucleation of $PtSn_2$ is complete, it grows primarily by expanding laterally without forming an intermediate phase. Two distinct morphologies of the propagation front are observed: diffuse (incomplete) and sharp (complete) edges (Figure 3c). While the incomplete edge shows gradual contrast variation across the boundary, the complete edge exhibits clear $PtSn_2\{112\}$ planes that terminate in SPS units at the boundary. The incomplete edge forms as a result of the in-plane atomic diffusion (Pt influx and Sn efflux), and those edges with an appropriate stoichiometry can be stabilized after formation of the $PtSn_2\{112\}$ planes. This distinct edge at the propagating front indicates the high stability of the $PtSn_2\{112\}$ planes, a characteristic that will be revisited in the following sections.

$PtSn_2$ to Pt_2Sn_3 (cubic to layered hexagonal) Phase Transformation. After further gradual heating to 500 °C (or slightly higher), a subsequent $PtSn_2$ to Pt_2Sn_3 phase transformation was observed. As discussed above (Figure 1a), the product Pt_2Sn_3 phase also has a layered structure but with narrower (1.814 Å) gaps between the $\{0001\}Pt_2Sn_3$ planes. In *in situ* experiments that examined this transition, pulse heating was applied to ensure the better thermal stability of the TEM holder and more consistent atomic-resolution STEM imaging (Figure S6 and Videos S4 and S5). This phase transformation is initiated via nucleation of Pt_2Sn_3 at the surfaces of $PtSn_2$ particles, after which the new Pt_2Sn_3 phases grow anisotropically through the parent material (Figure 4a and Video S4). In Figure 4b, two sequential atomic-resolution HAADF-STEM images show the growth of one new layer of Pt_2Sn_3 at the boundary between $PtSn_2$ and Pt_2Sn_3. The growth direction of the new phase is $Pt_2Sn_3\langle 1\bar{1}00\rangle$, which is one of the in-plane directions of Pt_2Sn_3.

The crystallographic OR of the $PtSn_2$ to Pt_2Sn_3 transformation was analyzed using CBED patterns and atomic-resolution STEM images as $PtSn_2\{112\}\|Pt_2Sn_3\{0001\}$ and $PtSn_2\langle 110\rangle\|Pt_2Sn_3\langle 2\bar{1}\bar{1}0\rangle$ (Figure S6). This crystallographic OR can be better understood in terms of the structural similarity between the two phases. The layer of Pt_2Sn_3 ($Pt_2Sn_3\{0001\}$) is comprised of an array of V-shaped structural units made of two tilted SPS units (labeled p and t in Figure 4b). One side of the layer (p side) forms a structure almost identical (except for a minor lattice mismatch of $\Delta d_{\text{in-plane}} = 4.9\%$) to the $PtSn_2\{112\}$ plane, which is a stable facet of $PtSn_2$

https://doi.org/10.1021/acs.nanolett.3c02162
Nano Lett. 2023, 23, 7576−7583

as discussed above (Figure 3c) [$\Delta d_{\text{in-plane}} = (d_{\text{PtSn2}\langle 110\rangle} - d_{\text{Pt}_2\text{Sn}_3\langle 2\bar{1}\bar{1}0\rangle})/d_{\text{PtSn}_2\langle 110\rangle}$]. Consequently, a stable semicoherent interface of $Pt_2Sn_3\{0001\}//PtSn_2\{112\}$ with misfit dislocations is produced. The phase transformation progresses in the direction parallel to the interface, preserving the semicoherent state (Video S5).

Two types of edge dislocations are frequently observed at this interface: one located at the propagation front of Pt_2Sn_3 with a Burgers vector perpendicular to the interface (type 1) and the second with a Burgers vector parallel to the interface (type 2) (Figure 4c). In type 1 dislocations, a single interfacial $PtSn_2\{112\}$ layer from the parent phase splits into two SPS layers of $Pt_2Sn_3\{0001\}$. The splitting is accompanied by reorientation of the p-type SPS in $PtSn_2$ to the t-type configuration, resulting in Pt_2Sn_3. The type 2 dislocations, which originate from the in-plane lattice mismatch between the $PtSn_2\{110\}$ and $Pt_2Sn_3\{2110\}$ planes at the interface, are misfit dislocations. Both dislocations play critical roles in the transformation of $PtSn_2$ into Pt_2Sn_3.

At the type 1 dislocations, the Pt atom at the middle of each SPS in the $PtSn_2\{112\}$ layer moves to the nearby sites between two Sn atoms, splitting one $Pt\{112\}_{PtSn_2}$ atomic plane into two planes and producing new t-type SPS units (step α in Figure 4d). Next, the two layers of the t-type SPS units relax and form the $Pt_2Sn_3\{0001\}$ layers. The additional Pt needed to fill the new Pt sites and to form Pt_2Sn_3 diffuses in parallel to the $Pt_2Sn_3\{0001\}$ layers, leaving Pt-depleted regions that can be readily observed as dark patches near the interface (Figure S6). Similar to the $PtSn_4$ to $PtSn_2$ phase transformation, the propagation and atomic rearrangements are highly anisotropic following the layered structure. The type 2 misfit dislocation drives flipping of the SPS unit between p and t (Figure 4c). The tensile strain in the $PtSn_2$ side produces an open space for easier atomic movement, resulting in flipping of the SPS unit and influx of Pt. Dislocation-guided transformations between two solid phases has been observed in other systems.[8−10] These observations, highlighted by the alignments of the SPS layers, again point to a dominant role of the structural characteristics of the parent and product phases in facilitating diffusive transformation.

Different from the cases discussed above, phase transformations from cubic $PtSn_2$ to hexagonal PtSn, where neither the parent phase nor the product phase has well-defined anisotropic structural characteristics, occur isotropically (section S2), further supporting the critical role of the lattice structure in the atomistic mechanisms of phase transformations. Our results demonstrate that solid to solid phase transformations follow a pathway that lies structurally between the parent and product phases, and the anisotropy in their lattice structures plays the most significant role in determining the atomic pathway. Atomic planes parallel to layers in a structure provide natural pathways for a facile elemental diffusion, and the gaps between the layers act as a buffer for local atomic modulations and rearrangements.

CONCLUSION

Our analysis of diffusive solid to solid phase transformations in the Pt−Sn system, based on direct atomic-resolution *in situ* STEM characterization, details how the relationship between the crystal structures of the parent and product phases dictates the atomistic mechanisms of the phase transformation. In the $PtSn_4$ to $PtSn_2$ phase transformation, in which highly anisotropic $PtSn_4$ with a layered structure transforms into isotropic $PtSn_2$ with a cubic structure, the transformation is initiated at 150 °C by forming a 2D periodic prestructure guided by the symmetry of the parent $PtSn_4$. Upon further heating to ∼200 °C, nucleation of an intermediate structure takes place following the prestructure. Next, the intermediate structure transforms into $PtSn_2$ and propagates in $PtSn_4$. The resulting slab of $PtSn_2$ with a thickness of 1.5 unit cells is coherently surrounded by the parent $PtSn_4$ phase. These atomic movements and rearrangements are driven by two structural factors: the presence of coherent planes at the interface of $PtSn_4$ and $PtSn_2$ and the high stability and flexibility of layered structures in $PtSn_4$. In the $PtSn_2$ to Pt_2Sn_3 phase transformation, where higher-symmetry $PtSn_2$ with a cubic structure transforms into lower-symmetry Pt_2Sn_3 with a layered structure at ≳500 °C, the transformation initiated on the surfaces propagates anisotropically along the in-plane direction of the layers of Pt_2Sn_3 mediated by the dislocations. Here again, the presence of a semicoherent interface between the phases and the stability and flexibility of the layered structure of the product Pt_2Sn_3 phase drive the atomic movements and rearrangements. Future computational studies investigating the energetics of the atomic planes and their strain dependency will help to improve our understanding of these observations. In the $PtSn_2$ to PtSn phase transformation, in which both parent and product phases are isotropic, the atomic movements and rearrangements are also isotropic without the formation of clearly defined interfacial structures.

The observed atomistic mechanisms of these transformations exhibit a clear correlation with the structural characteristics of the parent and product phases. Structural anisotropy in one of the involved phases can dictate a directional phase transformation due to the easy formation of stable habit planes, facile diffusion pathways, and structural flexibility. These results suggest that more research into examining the atomistic mechanisms of solid to solid phase transformations should be conducted to fully elucidate the principles of solid-state reactions and guide the efficient engineering of nanomaterials through phase transformation.

ASSOCIATED CONTENT

Supporting Information

The Supporting Information is available free of charge at https://pubs.acs.org/doi/10.1021/acs.nanolett.3c02162.

Methods; structure of the as-grown Pt_xSn_y films (section S1); crystal structures of the $PtSn_2$, Pt_2Sn_3, and PtSn phases (Figure S1); CBED map and atomic models at the major zone axes of all four Pt_xSn_y compounds (Figure S2); low-loss EELS obtained from the four Pt_xSn_y phases (Figure S3); supporting data for the $PtSn_4$ to $PtSn_2$ phase transformation (Figure S4); STEM images of the periodic feature and the intermediate phase in the $PtSn_4$ to $PtSn_2$ transition (Figure S5); supporting data for the Pt_2Sn_3 to $PtSn_2$ phase transformation (Figure S6); supporting data for the $PtSn_2$ to PtSn phase transformation (Figures S7 and S8); and details of the $PtSn_2$ to PtSn phase transformation (section S2) (PDF)

Video S1 (MP4)

Video S2 (MP4)

Video S3 (MP4)

Video S4 (MP4)

https://doi.org/10.1021/acs.nanolett.3c02162
Nano Lett. 2023, 23, 7576−7583

Video S5 (MP4)
Video S6 (MP4)

AUTHOR INFORMATION

Corresponding Authors

Hwanhui Yun − *Chemical Engineering and Materials Science, University of Minnesota, Twin Cities, Minneapolis, Minnesota 55455, United States; Korea Research Institute of Chemical Technology, Daejeon 34114, Korea*; Email: yunxx133@umn.edu

K. Andre Mkhoyan − *Chemical Engineering and Materials Science, University of Minnesota, Twin Cities, Minneapolis, Minnesota 55455, United States*; orcid.org/0000-0003-3568-5452; Email: mkhoyan@umn.edu

Authors

Delin Zhang − *Electrical Engineering and Computer Science, University of Minnesota, Twin Cities, Minneapolis, Minnesota 55455, United States*

Turan Birol − *Chemical Engineering and Materials Science, University of Minnesota, Twin Cities, Minneapolis, Minnesota 55455, United States*; orcid.org/0000-0001-5174-3320

Jian-Ping Wang − *Electrical Engineering and Computer Science, University of Minnesota, Twin Cities, Minneapolis, Minnesota 55455, United States*; orcid.org/0000-0002-0687-3203

Complete contact information is available at: https://pubs.acs.org/10.1021/acs.nanolett.3c02162

Author Contributions

H.Y. and K.A.M. conceived the project. H.Y. performed STEM experiments with input from K.A.M. D.Z. grew Pt−Sn thin films with input from J.-P.W. T.B. contributed to analysis. H.Y. and K.A.M. prepared the manuscript with contributions from all authors. K.A.M. directed all aspects of the project.

Notes

The authors declare no competing financial interest.

ACKNOWLEDGMENTS

This work was in part supported by SMART, one of seven centers of nCORE, a Semiconductor Research Corp. program, sponsored by the National Institute of Standards and Technology (NIST), the National Science Foundation (NSF) through Grant DMR-2309431, and the University of Minnesota MRSEC under Grant DMR-2011401 (seed). H.Y. would like to acknowledge institutional research program (KK2352-20) and support program for young researchers (BSK23-453) funded by KRICT. This work was carried out at the University of Minnesota (UMN) Characterization Facility, supported in part by the NSF through the UMN MRSEC program. The authors thank Prof. R. James and Dr. M. Odlyzko for fruitful discussions.

REFERENCES

(1) Chen, J. H.; Costan, E.; van Huis, M. A.; Xu, Q.; Zandbergen, H. W. Atomic pillar-Based Nanoprecipitates Strengthen AlMgSi Alloys. *Science* **2006**, *312*, 416.

(2) Shao, Z.; Cao, X.; Luo, H.; Jin, P. Recent progress in the phase-transition mechanism and modulation of vanadium dioxide materials. *NPG Asia Mater.* **2018**, *10*, 581.

(3) Zheng, Y.-R.; et al. Doping-induced structural phase transition in cobalt diselenide enables enhanced hydrogen evolution catalysis. *Nat. Commun.* **2018**, *9*, 2533.

(4) Usman, A.; Xiong, F.; Aftab, W.; Qin, M.; Zou, R. Emerging solid-to-solid phase-change materials for thermal-energy harvesting, storage, and utilization. *Adv. Mater.* **2022**, *34*, 2202457.

(5) Waitz, T.; Kazykhanov, V.; Karnthaler, H. P. Martensitic phase transformations in nanocrystalline NiTi studied by TEM. *Acta Mater.* **2004**, *52*, 137.

(6) Lu, N.; et al. Electric-field control of tri-state phase transformation with a selective dual-ion switch. *Nature* **2017**, *546*, 124.

(7) Li, W.; Qian, X.; Li, J. Phase transitions in 2D materials. *Nat. Rev. Mater.* **2021**, *6*, 829.

(8) Porter, D. A.; Easterling, K. E. *Phase transformations in metals and alloys*; CRC Press: Boca Raton, FL, 2009.

(9) Zhang, M.-X.; Kelly, P. M. Crystallographic features of phase transformations in solids. *Prog. Mater. Sci.* **2009**, *54*, 1101.

(10) Soffa, W. A.; Laughlin, D. E. 8. Diffusional phase transformations in the solid state. In *Physical Metallurgy*, 5th ed.; Laughlin, D. E., Hono, K., Eds.; Elsevier: Oxford, U.K., 2014; pp 851−1020.

(11) Denquin, A.; Naka, S. Phase transformation mechanisms involved in two-phase TiAl-based alloys—I. Lambellar structure formation. *Acta Mater.* **1996**, *44*, 343.

(12) Massalski, T. B.; Laughlin, D. E.; Soffa, W. A. The nature and role of incoherent interphase interfaces in diffusional solid-solid phase transformations. *Metall. Mater. Trans. A* **2006**, *37*, 825.

(13) Marioara, C. D.; Lefebvre, W.; Andersen, S. J.; Friis, J. Atomic structure of hardening precipitates in an Al−Mg−Zn−Cu alloy determined by HAADF-STEM and first-principles calculations: relation to η-$MgZn_2$. *J. Mater. Sci.* **2013**, *48*, 3638.

(14) Ha, D.-H.; et al. Solid−Solid Phase Transformations Induced through Cation Exchange and Strain in 2D Heterostructured Copper Sulfide Nanocrystals. *Nano Lett.* **2014**, *14*, 7090.

(15) Gao, P.; et al. Atomic-scale tracking of a phase transition from spinel to rocksalt in lithium manganese oxide. *Chem. Mater.* **2017**, *29*, 1006.

(16) Chung, T.-F.; et al. An atomic scale structural investigation of nanometre-sized η precipitates in the 7050 aluminium alloy. *Acta Mater.* **2019**, *174*, 351.

(17) Jin, H.; et al. Atomistic mechanism of phase transformation between topologically close-packed complex intermetallics. *Nat. Commun.* **2022**, *13*, 2487.

(18) Zhu, Y.; Yuan, D.; Zhang, H.; Xu, T.; Sun, L. Atomic-scale insights into the formation of 2D crystals from in situ transmission electron microscopy. *Nano Res.* **2021**, *14*, 1650.

(19) Zhu, S.-C.; Xie, S. -H; Liu, Z.-P. Nature of rutile nuclei in anatase-to-rutile phase transition. *J. Am. Chem. Soc.* **2015**, *137*, 11532.

(20) Ma, T.; et al. Toward phase and catalysis control: Tracking the formation of intermetallic nanoparticles at atomic scale. *Chem.* **2019**, *5*, 1235.

(21) Zandbergen, H. W.; Andersen, S. J.; Jansen, J. Structure determination of Mg_5Si_6 particles in Al by dynamic electron diffraction studies. *Science* **1997**, *277*, 1221.

(22) Yu, Q.; et al. In situ observation on dislocation-controlled sublimation of Mg nanoparticles. *Nano Lett.* **2016**, *16*, 1156.

(23) Zheng, X.; et al. Deformation induced FCC lamellae and their interaction in commercial pure Ti. *Scr. Mater.* **2019**, *162*, 326.

(24) DeSario, D. Y.; DiSalvo, F. J. Ordered intermetallic Pt−Sn nanoparticles: Exploring ordering behavior across the bulk phase diagram. *Chem. Mater.* **2014**, *26*, 2750.

(25) Cui, S.; Wang, J.; Jung, I.-H. Thermodynamic Assessments of the Pd−Sn and Pt−Sn systems with the modified quasi-chemical model for liquid. *Metall. Mater. Trans. A* **2022**, *53*, 4296.

(26) Aramesh, N.; et al. PtSn nanoalloy thin films as anode catalysts in methanol fuel cells. *Inorg. Chem.* **2020**, *59*, 10688.

(27) Liu, Z.; Jackson, G. S.; Eichhorn, B. W. PtSn Intermetallic, core−shell, and alloy nanoparticles as CO-tolerant electrocatalysts for H_2 oxidation. *Angew. Chem., Int. Ed.* **2010**, *49*, 3173.

(28) Li, G.; et al. Dirac nodal arc semimetal $PtSn_4$: An ideal platform for understanding surface properties and catalysis for hydrogen evolution. *Angew. Chem., Int. Ed.* **2019**, *58*, 13107.

(29) Motagamwala, A. H.; Almallahi, R.; Wortman, J.; Igenegbai, V. O.; Linic, S. Stable and selective catalysts for propane dehydrogenation operating at thermodynamic limit. *Science* **2021**, *373*, 217. Fu, X.; et al. Atomic-scale observation of non-classical nucleation-mediated phase transformation in a titanium alloy. *Nat. Mater.* **2022**, *21*, 290.
(30) Zhang, D.; et al. Robust negative longitudinal magnetoresistance and spin−orbit torque in sputtered Pt_3Sn and $Pt_3Sn_xFe_{1-x}$ topological semimetal. *Nat. Commun.* **2023**, *14*, 4151.
(31) $PtSn_4$ Crystal Structure: Datasheet from "PAULING FILE Multinaries ed." In *SpringerMaterials*; Springer-Verlag, Material Phases Data System (MPDS), and National Institute for Materials Science (NIMS), 2012.
(32) Pt_2Sn_3 Crystal Structure: Datasheet from "PAULING FILE Multinaries ed." *SpringerMaterials*; Springer-Verlag, Material Phases Data System (MPDS), and National Institute for Materials Science (NIMS), 2022.
(33) Peng, H.; Xie, C.; Schoen, D. T.; Cui, Y. Large anisotropy of electrical properties in layer-structured In_2Se_3 nanowires. *Nano Lett.* **2008**, *8*, 1511.
(34) $PtSn_2$ Crystal Structure: Datasheet from "PAULING FILE Multinaries ed." In *SpringerMaterials*; Springer-Verlag, Material Phases Data System (MPDS), and National Institute for Materials Science (NIMS), 2012.

https://doi.org/10.1021/acs.nanolett.3c02162
Nano Lett. 2023, 23, 7576−7583